

# Active interference suppression in frequency-division-multiplexed quantum gates via off-resonant microwave tones

Haruki Mitarai<sup>✉,†</sup>, Yukihiko Tadokoro<sup>✉,†</sup> and Hiroya Tanaka<sup>✉,‡</sup>

*Toyota Central R&D Labs., Inc., 41-1, Yokomichi, Nagakute, Aichi 480-1192, Japan*

(Dated: January 22, 2026)

An increase in the number of control lines between the quantum processors and the external electronics constitutes a major bottleneck in the realization of large-scale quantum computers. Frequency-division multiplexing is expected to enable multiple qubits to be controlled through a single microwave cable; however, interference from off-resonant microwave tones hinders precise qubit control. Here, we propose an active interference suppression method for frequency-division-multiplexed simultaneous gate operations. We demonstrate that deliberate incorporation of off-resonant microwave tones improves the accuracy of single-qubit gates. Specifically, we find that by incorporating off-resonant orthogonal or quasi-orthogonal microwave tones, the gate infidelity decreases proportionally to the inverse square of the number of microwave tones. Furthermore, we show that fast oscillations neglected under the rotating wave approximation degrade gate fidelity, and that this degradation can be mitigated through optimized frequency allocation. Our approach is simple yet effective for improving the performance of frequency-division-multiplexed quantum gates.

## I. INTRODUCTION

In recent years, significant efforts have been directed towards developing fault-tolerant quantum computers (FTQC) [1–9] which have potential applications in prime factorization [10], linear system solvers [11], and computer-aided engineering [12]. Among various platforms, superconducting circuits are particularly promising, and quantum supremacy and error correction using surface codes have been demonstrated experimentally [13–15]. However, achieving quantum advantage on realistic problems is expected to require millions of qubits [16, 17]. Building an FTQC at such scales demands not only improved qubit performance but also substantial advances in the associated control electronics.

Currently, control architectures for solid-state quantum processors commonly generate microwave signals at room temperature [18–22]. These signals are routed to individual qubits in a dilution refrigerator through one-to-one coaxial cables. However, this wiring model does not scale: the number of required control lines grows with the number of qubits. Increasing the number of control wires not only adds hardware complexity and cost but also introduces additional heat loads through physical interconnections, thereby threatening the cooling capacity of the dilution refrigerator [19].

Hence, reducing wiring is critical for scaling quantum computing systems [23–27]. Frequency-division multiplexing (FDM) allows a single microwave cable to simultaneously control multiple qubits [28–30], thereby reducing the number of required control lines. However,

a microwave tone intended for one qubit is off-resonant with other simultaneously driven qubits and can induce unwanted crosstalk, thus hindering precise parallel gate operations [26, 31]. Suppressing these crosstalk effects is therefore essential for achieving high-fidelity gates in FDM schemes. Several studies combined FDM with cryogenic qubit controllers [22, 28, 29]. For example, a frequency-division-multiplexed qubit controller based on adiabatic quantum-flux-parametron logic was demonstrated [22]. Nevertheless, the development of cryogenic qubit controllers remains technically challenging. Recent work has explored pulse-spectral engineering, which can potentially circumvent these challenges [32, 33]. For instance, selective gate operations enabled by pulse shaping are demonstrated [32].

In this study, we propose an active interference suppression (AIS) for simultaneous gate operations in FDM schemes. Our proposal is motivated by the recent observations that the incorporation of appropriately chosen off-resonant tones can suppress interference [33]. We show that deliberate incorporation of off-resonant orthogonal or quasi-orthogonal frequency tones improves the single-qubit gate fidelity. Specifically, for qubits which are arranged at regular intervals in the frequency domain, gate infidelity decreases proportionally to the inverse square of the number of applied microwave tones. We further show that fast-oscillating terms neglected under the rotating wave approximation (RWA) can affect the gate fidelity in the AIS method. By shifting the center frequency of off-resonant microwave tones, we compensate for this effect and achieve higher fidelity.

AIS provides an alternative perspective on the common view that off-resonant microwave tones are harmful to qubit control. Our results are consistent with recent work that highlights the constructive role of carefully engineered off-resonant components [33, 34]. Moreover, the applicability of our framework is not limited to FDM-based simultaneous gate operations. It can be readily

\* [hmitarai@mosk.tylabs.co.jp](mailto:hmitarai@mosk.tylabs.co.jp)

† [y.tadokoro@ieee.org](mailto:y.tadokoro@ieee.org)

‡ [tanak@mosk.tylabs.co.jp](mailto:tanak@mosk.tylabs.co.jp)

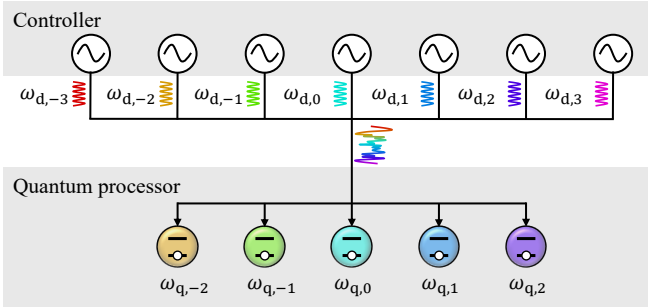


FIG. 1. Conceptual illustration of a model consisting of  $N_q$  independent qubits with frequencies  $\omega_{q,k_q}$  driven by microwaves via a shared control line. The controller produces  $N_d$  microwave tones at distinct frequencies  $\omega_{d,k_d}$ , which are then combined and routed to a quantum processor via the shared line. The combined signal is applied uniformly to all qubits. In this figure,  $N_q = 5$  and  $N_d = 7$ .

extended to other tasks in qubit manipulation, such as selective excitation [32] and microwave crosstalk mitigation [35].

## II. MODEL

### A. System Hamiltonian

Figure 1 illustrates a system of  $N_q$  independent qubits driven by a frequency-division-multiplexed microwave signal. The controller generates  $N_d$  microwave tones, which are combined and transmitted to the quantum processor through a shared control line. The synthesized signal is applied uniformly to all the qubits. The Hamiltonian of this system is given by

$$H_{\text{all}}(t) \equiv \sum_{k_q \in K_q} \left[ -\frac{\omega_{q,k_q}}{2} \sigma_{z,k_q} + \sum_{k_d \in K_d} \alpha_{k_d} s(t) \sin(\omega_{d,k_d} t + \theta_{k_d}) \sigma_{y,k_q} \right], \quad (1)$$

where  $\omega_{d,k_d}$ ,  $\theta_{k_d}$ , and  $\alpha_{k_d}$  denote the frequency, phase, and amplitude, respectively, of the  $k_d$ th microwave tone. The resonance frequency of the  $k_q$ th qubit is  $\omega_{q,k_q}$ .  $K_q = \{l_q, l_q + 1, \dots, r_q - 1, r_q\}$  is the set of qubit indices with cardinality  $|K_q| = N_q = r_q - l_q + 1$  and  $K_d = \{l_d, l_d + 1, \dots, r_d - 1, r_d\}$  is the set of indices of drive microwave tones with  $|K_d| = N_d = r_d - l_d + 1$ . The integers  $l_q, l_d \leq 0$  and  $r_q, r_d \geq 0$  denote the left and right boundaries of the index set. The operators  $\sigma_{x,k_q}$ ,  $\sigma_{y,k_q}$  and  $\sigma_{z,k_q}$  are the Pauli operators associated with the  $k_q$ th qubit. The function  $s(t)$  represents the pulse envelope.

Since arbitrary single-qubit gates can be implemented using  $X$  and virtual- $Z$  gates [36], we consider only the driving terms involving  $\sigma_{y,k_q}$ . We now focus on the  $k_q$ th

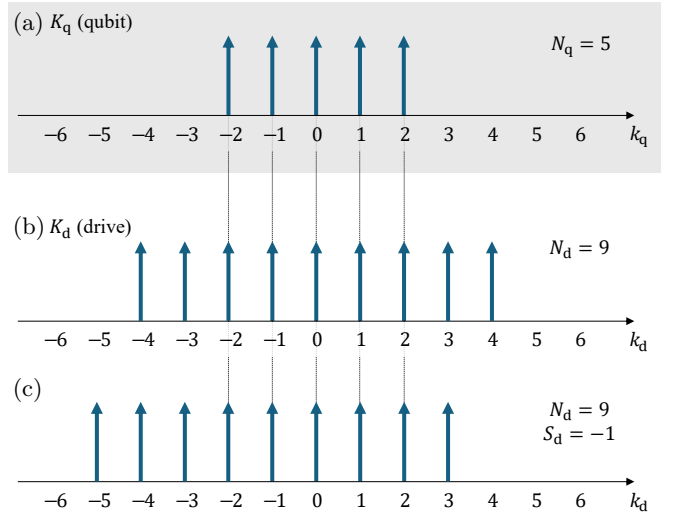


FIG. 2. Illustration of the set  $K_q$  and  $K_d$ . (a) Set of qubit indices  $K_q$  for  $N_q = 5$ ,  $l_q = -2$ , and  $r_q = 2$ . (b), (c) Set of indices of drive microwave tones  $K_d$  for  $N_d = 9$ . The set  $K_d$  shown in (b) corresponds to symmetric allocation, namely,  $l_d = -[N_d/2]$  and  $r_d = [(N_d - 1)/2]$ . The set shown in (c) corresponds to weakly asymmetric allocation, namely,  $l_d = -[N_d/2] + S_d$  and  $r_d = [(N_d - 1)/2] + S_d$  with  $S_d = -1$ . The shift parameter  $S_d$  is introduced to allow asymmetric allocation.

qubit in Eq. (1) and analyze its dynamics using the corresponding single-qubit Hamiltonian:

$$H(t) \equiv -\frac{\omega_{q,k_q}}{2} \sigma_{z,k_q} + \sum_{k_d \in K_d} \alpha_{k_d} s(t) \sin(\omega_{d,k_d} t) \sigma_{y,k_q}. \quad (2)$$

For simplicity, we set  $\theta_{k_d} = 0$  for all  $k_d$ . Equation (2) describes the dynamics of the  $k_q$ th qubit under a multiplexed microwave drive.

We allocate qubit frequencies  $\omega_{q,k_q}$  and drive frequencies  $\omega_{d,k_d}$  at regular intervals  $\Delta$ , where  $\Delta \ll \omega_{q,k_q}, \omega_{d,k_d}$ , and choose them such that  $\omega_{q,k_q} = \omega_{d,k_d}$  for  $k_q = k_d$ . This yields  $\omega_{d,k_d} = \omega_{q,k_q} + (k_d - k_q) \Delta$ . For convenience, we take  $r_q = -l_q = (N_q - 1)/2$  for odd  $N_q$ , and in what follows we consider only odd  $N_q$ . Figure 2(a) shows an example of such  $K_q$  for  $N_q = 5$ ,  $l_q = -2$ , and  $r_q = 2$ . In addition, we assume that  $s(t)$  is constant when the control is active, and set  $\alpha_{k_d} = \alpha$  for all  $k_d$ . Under these assumptions, the system Hamiltonian  $H_I$  in the frame that rotates at qubit frequency is given by

$$H_I(t) = \frac{\alpha}{2} s(t) \sum_{k_d \in K_d} \left[ \sigma_{x,k_q} \{ \cos((2\omega_{q,k_q} + \Delta_{k_d k_q}) t) - \cos(\Delta_{k_d k_q} t) \} + \sigma_{y,k_q} \{ \sin((2\omega_{q,k_q} + \Delta_{k_d k_q}) t) + \sin(\Delta_{k_d k_q} t) \} \right], \quad (3)$$

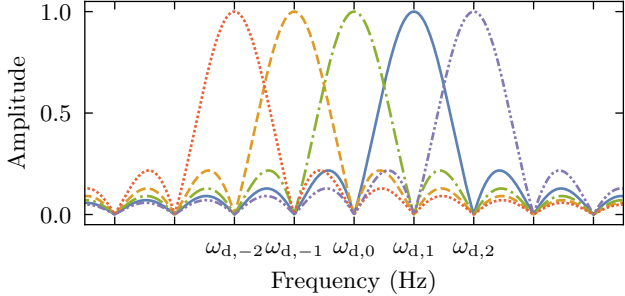


FIG. 3. Absolute values of the normalized spectra of  $s(t) \sin(\omega_{d,k_d} t)$  for  $k_d \in \{-2, -1, 0, 1, 2\}$  with  $\tau = \tau_0$ . Each drive frequency  $\omega_{d,k_d}$  is located at a zero crossing of the spectral components of all other microwave tones.

where  $\Delta_{kj} \equiv (k - j)\Delta$ ,

$$s(t) = \begin{cases} 1 & 0 \leq t \leq \tau \\ 0 & \text{otherwise} \end{cases}, \quad (4)$$

and  $\tau$  is the pulse width. Equation (3) can be simplified by applying the RWA:

$$H_1(t) \sim \frac{\alpha}{2} s(t) \sum_{k_d \in K_d} [-\sigma_{x,k_q} \cos(\Delta_{k_d k_q} t) + \sigma_{y,k_q} \sin(\Delta_{k_d k_q} t)]. \quad (5)$$

Equation (5) is used for the theoretical analysis in Sec. III.

## B. Orthogonal and quasi-orthogonal pulses

For the Hamiltonian given in Eq. (3), the gate fidelity improves at specific values of the pulse width  $\tau$ . In this context, we introduce orthogonal and quasi-orthogonal pulses [33].

The Fourier transform of the pulse  $s(t) \sin(\omega_{d,k_d} t)$  in Eq. (2) is proportional to a sinc function. This sinc function has zero crossings at regular intervals of  $2\pi/\tau$ , except at its center. For  $\tau = \tau_0$ , where  $\tau_0 \equiv 2\pi/\Delta$ , the spacing between adjacent zero crossings coincides with the drive and qubit frequency interval  $\Delta$ . Consequently, as shown in Fig. 3, the spectral peak of each microwave tone aligns with the nulls of all the other tones, thereby suppressing interference and yielding high gate fidelity [33]. This mechanism is conceptually analogous to orthogonal frequency-division multiplexing (OFDM) [37–39], which is widely used in wireless communication systems. Ref. [33] further showed that high gate fidelity is also achievable for  $\tau = \tau_0/2$ .

Similar fidelity improvements can be obtained for nonzero integer multiples of these pulse widths. Let  $m$  be a positive integer. We refer to pulses with widths  $\tau = m\tau_0/2$  as “orthogonal” when  $m$  is even and “quasi-orthogonal” when  $m$  is odd.

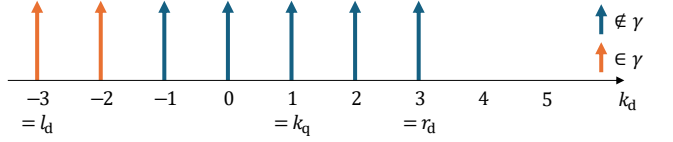


FIG. 4. Illustration of  $\gamma$ , which represents the set of indices of drive microwave tones lacking a corresponding element with respect to  $k_d = k_q$ . The orange and blue arrows denote the driving microwaves that correspond and do not correspond to the set  $\gamma$ , respectively. In this figure,  $k_q = 1$ ,  $l_d = -3$ , and  $r_d = 3$ , yielding  $\gamma = \{k_q - 3, k_q - 4\} = \{-2, -3\}$ . These indices have no counterpart related to  $k_q$ , i.e., there are no arrows at  $k_q + 3 = 4$  and  $k_q + 4 = 5$ .

## III. THEORY OF ACTIVE INTERFERENCE SUPPRESSION

The average gate fidelity  $F(U_1, U_2)$  is defined as [40]

$$F(U_1, U_2) \equiv \frac{|\text{Tr} (U_1^\dagger U_2)|^2 + d}{d(d+1)}, \quad (6)$$

where  $U_1$  and  $U_2$  are unitary operators and  $d$  is the dimension of the Hilbert space. To quantify the impact of interference on gate performance, we use the average gate infidelity  $1 - F(U_{\text{ideal}}, U)$ , where  $U_{\text{ideal}} \equiv e^{-i\frac{\phi}{2}\sigma_{x,k_q}}$  denotes the desired unitary operator with the rotation angle  $\phi$ . The operator  $U$  denotes the actual evolution operator defined as  $|\psi_I(\tau)\rangle = U|\psi_I(0)\rangle$ .

For an analytical estimate of the infidelity, we expand the time evolution operator via the Magnus expansion [41]. We define the resulting approximate operator  $U_{\text{Magnus}}$  as

$$U_{\text{Magnus}}(t) \equiv \exp[-i\{\Omega_1(t) + \Omega_2(t)\}], \quad (7)$$

where  $\Omega_1(t)$  and  $\Omega_2(t)$  are the first and second terms of the Magnus series. Using Eq. (5),  $\Omega_1(t)$  and  $\Omega_2(t)$  take the following forms [33]:

$$\Omega_1(t) \sim -(\sigma_{x,k_q}\lambda_x + \sigma_{y,k_q}\lambda_y), \quad (8)$$

$$\Omega_2(t) \sim -\sigma_{z,k_q}\lambda_z, \quad (9)$$

where  $\lambda_x$ ,  $\lambda_y$ , and  $\lambda_z$  are complex coefficients. Using Eqs. (7)–(9), the infidelity becomes [33]

$$1 - F(U_{\text{ideal}}, U_{\text{Magnus}}(\tau)) \sim 1 - \frac{1}{3} \left( 2 \left| \cos \left| \frac{\phi}{2} \right| \cos \Lambda - \frac{\phi \lambda_x}{|\phi| \Lambda} \sin \left| \frac{\phi}{2} \right| \sin \Lambda \right|^2 + 1 \right), \quad (10)$$

where  $\Lambda \equiv \sqrt{\lambda_x^2 + \lambda_y^2 + \lambda_z^2}$ . Thus,  $\lambda_x \sim -\phi/2$  and  $\lambda_y, \lambda_z \sim 0$  lead to high-fidelity gates.

We now introduce the AIS method and theoretically analyze its effects on gate infidelity. For orthogonal or quasi-orthogonal pulses, i.e.,  $\tau = m\tau_0/2$ , the coefficients  $\lambda_x$ ,  $\lambda_y$ , and  $\lambda_z$  become [33]

$$\lambda_x = -\frac{\phi}{2}, \quad (11)$$

$$\lambda_y = -\frac{\phi}{2\pi m} \sum_{k_d \in \gamma} \frac{(-1)^{m(k_d - k_q)} - 1}{k_d - k_q}, \quad (12)$$

$$\lambda_z = \frac{\phi^2}{4\pi m} \sum_{k_d \in \gamma} \frac{(-1)^{m(k_d - k_q)}}{k_d - k_q}. \quad (13)$$

Here, we set  $\alpha = -\phi/\tau$ , and  $\gamma \subseteq K_d$  denotes the set of indices of drive microwave tones lacking a corresponding element with respect to  $k_d = k_q$  (see Fig. 4). We clearly have  $\lambda_x = -\phi/2$ . However, nonzero  $\lambda_y$  and  $\lambda_z$  degrade the fidelity. In particular, gate operations on qubits near the left or right ends ( $k_q \sim l_d$  or  $k_q \sim r_d$ ) show lower fidelity due to the large cardinality  $|\gamma|$ .

To compensate for this reduction in fidelity, we introduce additional off-resonant drive tones. In Eqs. (12) and (13), the coefficients  $|\lambda_y|$  and  $|\lambda_z|$  take smaller values when (1) the cardinality  $|\gamma|$  is small or (2) the members of  $\gamma$  are far from the qubit index  $k_q$ . While condition (1) cannot be satisfied simultaneously across all qubits, condition (2) can be fulfilled by adding off-resonant tones symmetrically relative to the central qubit's frequency  $\omega_{q,0}$ . By choosing  $l_d = -\lfloor N_d/2 \rfloor$  and  $r_d = \lfloor (N_d - 1)/2 \rfloor$ , which corresponds to  $K_d$  shown in Fig. 2(b),  $|\lambda_y|$  and  $|\lambda_z|$  for  $N_d \gg |k_q|$  become

$$|\lambda_y| \sim \frac{|\phi|}{\pi m N_d} |\gamma| - G(k_q, m, \gamma), \quad (14)$$

$$|\lambda_z| \sim \frac{\phi^2}{2\pi m N_d} |G(k_q, m, \gamma)|, \quad (15)$$

where

$$G(k_q, m, \gamma) = \sum_{k_d \in \gamma} (-1)^{m(k_d - k_q)}. \quad (16)$$

Assuming  $\lambda_x = -\frac{\phi}{2}$  and  $|\lambda_y|, |\lambda_z| \ll |\lambda_x|$ , Eq. (10) reduces to

$$1 - F(U_{\text{ideal}}, U_{\text{Magnus}}(\tau)) \sim \frac{\lambda_y^2 + \lambda_z^2}{3\lambda_x^2}. \quad (17)$$

Thus, substituting Eqs. (11), (14), and (15) into Eq. (17), the infidelity can be rewritten as

$$\begin{aligned} 1 - F(U_{\text{ideal}}, U_{\text{Magnus}}(\tau)) \\ \sim \frac{1}{3\pi^2 m^2 N_d^2} \left[ 4 \{ |\gamma| - G(k_q, m, \gamma) \}^2 \right. \\ \left. + \phi^2 G^2(k_q, m, \gamma) \right]. \quad (18) \end{aligned}$$

Here,  $G(k_q, m, \gamma) = |\gamma|$  for even  $m$ , while for odd  $m$  it takes the values 0, -1, or 1. Additionally,  $|\gamma|$  differs by

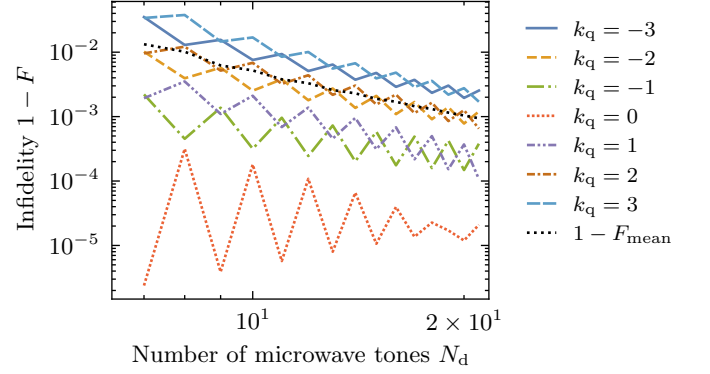


FIG. 5. Average gate infidelity  $1 - F(U_{\text{ideal}}, U)$  as a function of the number of drive microwave tones  $N_d$  for  $\tau = \tau_0$ . Parameters are set as  $N_q = 7$ ,  $l_q = -3$ ,  $r_q = 3$ ,  $l_d = -\lfloor N_d/2 \rfloor$ ,  $r_d = \lfloor (N_d - 1)/2 \rfloor$ ,  $\omega_{q,0}/2\pi = 5$  GHz,  $\Delta/2\pi = 10$  MHz,  $\phi = \pi/2$ , and  $\alpha = -\phi/\tau$ . The black dotted line indicates  $1 - F_{\text{mean}}(U_{\text{ideal}}, U)$ , which is the mean value of  $1 - F(U_{\text{ideal}}, U)$  over  $k_q \in K_q = \{-3, -2, -1, 0, 1, 2, 3\}$ . The operator  $U$  is obtained numerically from the Hamiltonian in Eq. (2).

only one depending on whether  $N_d$  is even or odd. Therefore, fixing  $m$  and  $k_q$ , the infidelity is expected to scale as  $N_d^{-2}$  when orthogonal or quasi-orthogonal microwave tones are incorporated.

#### IV. NUMERICAL RESULTS

In this section, we confirm the effectiveness of the AIS method introduced in Sec. III. We also identify the conditions on the pulse width required for AIS. For this purpose, we obtain the exact evolution operator  $U$  numerically from the Hamiltonian in Eq. (2).

##### A. Reduction of gate infidelity with AIS

Figure 5 shows the average gate infidelity  $1 - F(U_{\text{ideal}}, U)$  for each qubit as a function of the number of drive microwave tones  $N_d$ . We set  $\tau = \tau_0$  and  $N_q = 7$ . The black dotted line represents  $1 - F_{\text{mean}}(U_{\text{ideal}}, U)$ , the mean infidelity over all qubits  $k_q \in K_q$ . Here,  $F_{\text{mean}}(U_1, U_2) \equiv \frac{1}{N_q} \sum_{k_q \in K_q} F(U_1, U_2)$ . In Fig. 5, we find that the infidelity decreases as  $N_d$  increases. Fitting a linear function to the black dotted line in the range  $11 \leq N_d \leq 21$ , we obtain a slope of approximately -2.2. This result is consistent with the scaling predicted by Eq. (18), which indicates the infidelity decreases proportionally to  $N_d^{-2}$ . Here, data for  $N_d < 11$  is excluded since Eq. (18) assumes  $N_d \gg |k_q|$ . The jagged features of the infidelity curves reflect changes in  $|\gamma|$ , which differs by one between even and odd values of  $N_d$ .

Note that, for  $k_q = 0$ , the theoretical infidelity  $1 - F(U_{\text{ideal}}, U_{\text{Magnus}}(\tau))$ , given by Eq. (10), vanishes when

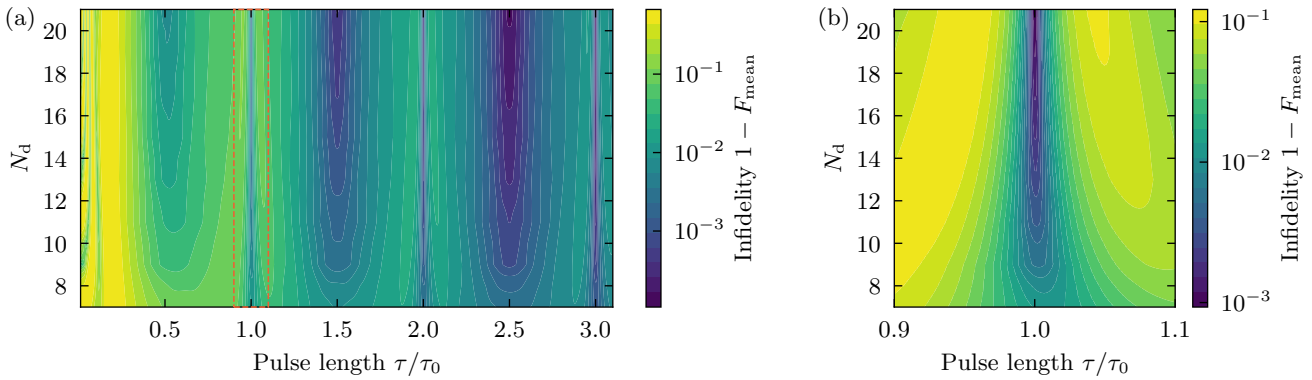


FIG. 6. (a) Infidelity  $1 - F_{\text{mean}}(U_{\text{ideal}}, U)$  as a function of the number of drive microwave tones  $N_d$  and the normalized pulse width  $\tau/\tau_0$  for  $0.01 \leq \tau/\tau_0 \leq 3.1$ . (b) Enlarged view of (a) in the range  $0.9 \leq \tau/\tau_0 \leq 1.1$ , corresponding to the region outlined by the orange dashed lines. Parameters are:  $N_q = 7$ ,  $l_q = -3$ ,  $r_q = 3$ ,  $l_d = -\lfloor N_d/2 \rfloor$ ,  $r_d = \lfloor (N_d-1)/2 \rfloor$ ,  $\omega_{q,0}/2\pi = 5 \text{ GHz}$ ,  $\Delta/2\pi = 10 \text{ MHz}$ ,  $\phi = \pi/2$ , and  $\alpha = -\phi/\tau$ .  $F_{\text{mean}}(U_{\text{ideal}}, U)$  denotes the mean of  $F(U_{\text{ideal}}, U)$  over all qubits  $k_q \in K_q = \{-3, -2, -1, 0, 1, 2, 3\}$ . The operator  $U$  is obtained numerically from the Hamiltonian in Eq. (2).

$N_d$  is odd because the coefficients in Eqs. (11)–(13) satisfy  $\lambda_x = -\phi/2$ ,  $\lambda_y = 0$ , and  $\lambda_z = 0$ . However, the numerical value  $1 - F(U_{\text{ideal}}, U)$  remains nonzero, as shown in Fig. 5. This discrepancy arises from the RWA employed to derive  $1 - F(U_{\text{ideal}}, U_{\text{Magnus}}(\tau))$ . The fast-oscillating terms neglected under the RWA cause residual crosstalk in the numerical evolution, resulting in a nonzero value of the infidelity  $1 - F(U_{\text{ideal}}, U)$ .

## B. Pulse width requirements for AIS

We now present the pulse width requirements for AIS. Figure 6(a) shows the infidelity  $1 - F_{\text{mean}}(U_{\text{ideal}}, U)$  as a function of the number of drive microwave tones  $N_d$  and the normalized pulse width  $\tau/\tau_0$ . Figure 6(b) is an enlarged view of Fig. 6(a) in the range  $0.9 \leq \tau/\tau_0 \leq 1.1$ , corresponding to the region outlined by the orange dashed lines. For  $\tau = m\tau_0/2$ , i.e., in the orthogonal and quasi-orthogonal cases, the infidelity decreases as  $N_d$  increases; thus AIS has a beneficial effect. This result is consistent with the analytical prediction in Sec. III. However, for  $\tau \neq m\tau_0/2$ , the infidelity remains almost constant over the entire range of  $N_d$ . This is because, in this case, the unwanted terms do not vanish and thus limit the effectiveness of AIS (see Appendix A).

This result significantly restricts the allowable values of  $\tau$ . However,  $\tau$  is originally chosen from the set  $\{m\tau_0/2\}$  to achieve high fidelity [33]. Therefore, this restriction does not constitute a significant limitation of AIS.

## V. COMPENSATING FOR EFFECTS OF FAST-OSCILLATING TERMS

In this section, we numerically demonstrate that fast-oscillating terms degrade the overall gate fidelity. While

Eqs. (10)–(13) show that infidelity for  $\tau = m\tau_0/2$  and  $l_d = -r_d$  is symmetric about  $k_q = 0$  under the RWA, this symmetry is broken beyond the RWA. Specifically, terms involving  $2\omega_{q,k_q} + \Delta_{k_d k_q}$  in Eq. (3) introduce a slight asymmetry, leading to a degradation of the overall gate fidelity. We consequently show that fine-tuning of the drive frequency allocation can compensate for this effect and improve overall performance.

## A. Dependence on the qubit frequency

In Fig. 7(a), we plot the infidelity  $1 - F(U_{\text{ideal}}, U)$  as a function of the qubit index  $k_q$  for  $\omega_{q,0}/2\pi = 1$ , 2.5, and 5 GHz. We set  $N_q = 7$  and  $N_d = 21$ , and we place the microwave tones symmetrically with respect to the central qubit  $k_q = 0$ , such that  $-l_d = r_d$ . The evolution operator  $U$  is obtained numerically from the Hamiltonian in Eq. (2). Notably, the infidelity is asymmetric about  $k_q = 0$ ; the infidelity for negative  $k_q$  is larger than that for positive  $k_q$ . Therefore, we expect the mean infidelity over  $k_q \in K_q$  to decrease when the centroid of the microwave tones is shifted slightly towards lower frequencies. In addition, this asymmetry increases as  $\omega_{q,0}$  decreases; therefore, a larger shift is required for smaller  $\omega_{q,0}$ .

Figure 7(b) shows the infidelity  $1 - F_{\text{mean}}(U_{\text{ideal}}, U)$  as a function of the shift  $S_d$  and  $\omega_{q,0}/2\pi$  for  $N_q = 7$  and  $N_d = 21$ . Here,  $S_d$  is introduced to allow asymmetric allocation. The microwave tones are symmetrically allocated with respect to  $k_d = S_d$ ; accordingly,  $l_d = -\lfloor N_d/2 \rfloor + S_d$ ,  $r_d = \lfloor (N_d-1)/2 \rfloor + S_d$  [see Fig. 2(c) for an example with  $N_d = 9$  and  $S_d = -1$ ]. Cross symbols correspond to the minimal infidelity for each value of  $\omega_{q,0}$ . The shifts yielding minimal infidelity move to the left as  $\omega_{q,0}$  decreases. Specifically, for  $\omega_{q,0}/2\pi = 1$ , 1.5, and 2 GHz, we see the minimal infidelity at  $S_d = -1$ ,

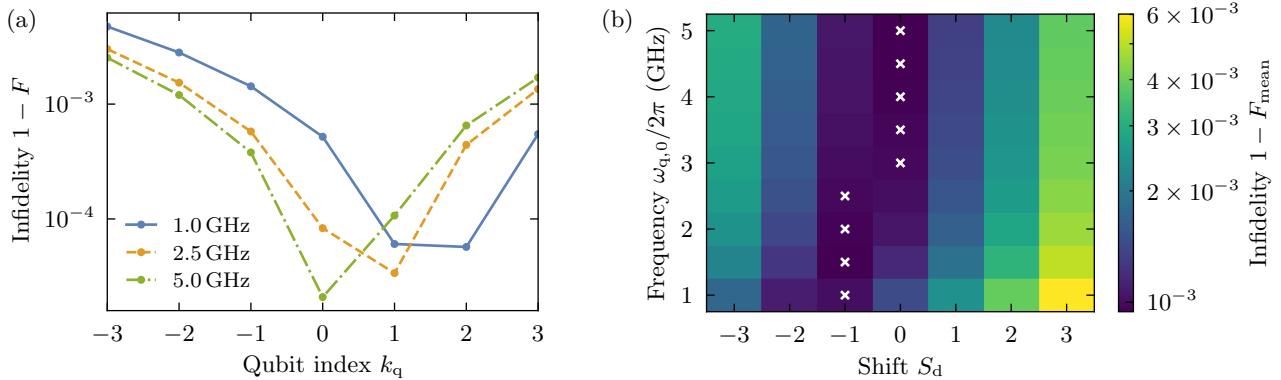


FIG. 7. (a) Infidelity  $1 - F(U_{\text{ideal}}, U)$  as a function of the qubit index  $k_q$  for  $S_d = 0$ , where three curves are shown for  $\omega_{q,0}/2\pi = 1, 2.5$ , and  $5$  GHz. (b) Infidelity  $1 - F_{\text{mean}}(U_{\text{ideal}}, U)$  as a function of the microwave tone shift  $S_d$  and the central qubit frequency  $\omega_{q,0}$ .  $F_{\text{mean}}(U_{\text{ideal}}, U)$  denotes the mean of  $F(U_{\text{ideal}}, U)$  over all qubits  $k_q \in K_q = \{-3, -2, -1, 0, 1, 2, 3\}$ . Parameters are:  $N_q = 7$ ,  $l_q = -3$ ,  $r_q = 3$ ,  $N_d = 21$ ,  $l_d = -\lfloor N_d/2 \rfloor + S_d$ ,  $r_d = \lfloor (N_d - 1)/2 \rfloor + S_d$ ,  $\Delta/2\pi = 10$  MHz,  $\phi = \pi/2$ ,  $\tau = \tau_0$ , and  $\alpha = -\phi/\tau$ . In (b), local minima of infidelity for each  $\omega_{q,0}$  are plotted with crosses. The operator  $U$  is obtained numerically from the Hamiltonian in Eq. (2).

while it is given at  $S_d = 0$  for  $\omega_{q,0}/2\pi \geq 2.5$  GHz. For  $\omega_{q,0}/2\pi = 1$  GHz, we observe a reduction in the mean infidelity  $1 - F_{\text{mean}}(U_{\text{ideal}}, U)$  from  $1.45 \times 10^{-3}$  at  $S_d = 0$  to  $1.01 \times 10^{-3}$  at  $S_d = -1$ , a 30.3% decrease.

### B. Dependence on the number of drive tones

The number of drive microwave tones  $N_d$  also affects the optimal value of the shift  $S_d$ . Figure 8(a) shows the infidelity as a function of the qubit index  $k_q$  for  $N_d = 7, 19$ , and  $31$ . We set  $N_q = 7$  and place the microwave tones symmetrically with respect to the central qubit  $k_q = 0$ , as in Fig. 7(a). The asymmetry of the infidelity about  $k_q = 0$  increases for larger  $N_d$ . This behavior arises because the contributions of the terms neglected under the RWA (associated with  $2\omega_{q,k_q} + \Delta_{k_d k_q}$ ) accumulate over all drive microwave tones. Therefore, a larger shift is required for larger  $N_d$  to compensate for the increased asymmetry and thereby improve the mean fidelity over all qubits.

Figure 8(b) shows the mean gate infidelity  $1 - F_{\text{mean}}(U_{\text{ideal}}, U)$  as a function of the shift  $S_d$  and the number of drive microwave tones  $N_d$ . The optimal shift for each  $N_d$ , plotted with a cross, tends to move to the left as  $N_d$  increases. Notably, for  $N_d = 31$ , we obtain a mean infidelity of  $4.39 \times 10^{-4}$  at  $S_d = -2$ , a 52.3% reduction compared to  $9.22 \times 10^{-4}$  at  $S_d = 0$ .

## VI. DISCUSSION

In Sec. V we have shown that infidelity can be reduced by taking into account the effects neglected under the RWA. When  $N_d = 1$ , which is a typical value for conventional one-to-one wiring systems, the contributions of fast-oscillating terms to the fidelity are negligible because

they are several orders of magnitude smaller than those of the resonant terms. However, as  $N_d$  increases, these contributions accumulate over all the drive microwave tones. Therefore, their impact on gate performance must be considered when adopting AIS, which uses a large number of drive microwave tones.

We have not considered nonadiabatic transitions and leakage outside the computational subspace to isolate and clarify the essential physics of the AIS method. A possible measure to suppress such leakage is to replace the edges of the rectangular pulse envelope with a raised cosine envelope, and to employ derivative removal by adiabatic gate (DRAG) pulses [42, 43]. Furthermore, the allowable values of  $N_d$  and  $N_q$  are limited by the frequency spacing  $\Delta$  to avoid spectral overlap with the leakage transition frequency. This constraint represents a limitation of our approach.

## VII. CONCLUSION

In this paper, we have presented an active interference suppression method for simultaneous gate operations based on the OFDM scheme. We have demonstrated a reduction in the infidelity of single-qubit gates by deliberately incorporating off-resonant orthogonal or quasi-orthogonal microwave tones. Notably, we have shown analytically and numerically that this reduction is approximately proportional to the inverse square of the number of incorporated microwave tones.

Further, we have shown that fast-oscillating terms neglected under the RWA affect gate fidelity. By shifting the centroid of the off-resonant microwave tones in the frequency domain, we mitigated this effect and achieved higher fidelity.

We have focused on simultaneous gate operations

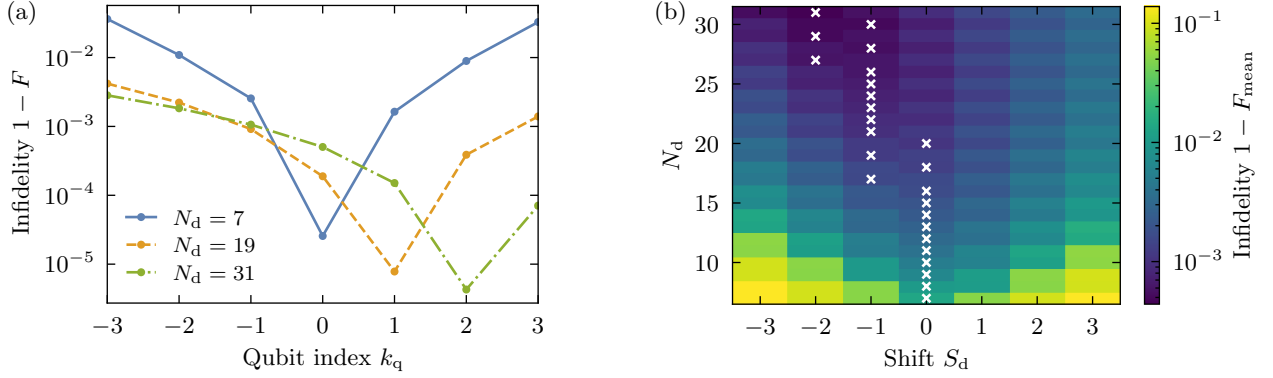


FIG. 8. (a) Infidelity  $1 - F(U_{\text{ideal}}, U)$  as a function of the qubit index  $k_q$  for  $S_d = 0$ , where three curves are shown for  $N_d = 7, 19$ , and  $31$ . (b) Infidelity  $1 - F_{\text{mean}}(U_{\text{ideal}}, U)$  as a function of the microwave-tone shift  $S_d$  and the number of drive microwave tones  $N_d$ .  $F_{\text{mean}}(U_{\text{ideal}}, U)$  is the mean of  $F(U_{\text{ideal}}, U)$  over all qubits  $k_q \in K_q = \{-3, -2, -1, 0, 1, 2, 3\}$ . Parameters are:  $N_q = 7$ ,  $l_q = -3$ ,  $r_q = 3$ ,  $l_d = -\lfloor N_d/2 \rfloor + S_d$ ,  $r_d = \lfloor (N_d - 1)/2 \rfloor + S_d$ ,  $\omega_{q,0}/2\pi = 1.5$  GHz,  $\Delta/2\pi = 10$  MHz,  $\phi = \pi/2$ ,  $\tau = \tau_0$ , and  $\alpha = -\phi/\tau$ . In (b), local minima of infidelity for each  $N_d$  are plotted with crosses. The evolution operator  $U$  is obtained numerically from the Hamiltonian in Eq. (2).

based on the FDM scheme. However, we expect that the concept of AIS can be applied to related control problems, such as selective excitation [32] or microwave crosstalk mitigation [35].

#### ACKNOWLEDGMENTS

This study used QuTiP [44] for numerical calculations.

#### Appendix A: Origin of the reduced effectiveness of AIS for $\tau \neq m\tau_0/2$

As shown in Sec. IV B, the effectiveness of AIS decreases for  $\tau \neq m\tau_0/2$ . In this appendix, we examine this behavior through the coefficients  $\lambda_x$ ,  $\lambda_y$ , and  $\lambda_z$  introduced in Eqs. (8) and (9).

The first and second terms of the Magnus series,  $\Omega_1(t)$

and  $\Omega_2(t)$ , introduced in Eq. (7), are given by

$$\Omega_1(t) \equiv \int_0^t H_I(t_1) dt_1, \quad (\text{A1})$$

$$\Omega_2(t) \equiv -\frac{i}{2} \int_0^t \int_0^{t_1} [H_I(t_1), H_I(t_2)] dt_2 dt_1. \quad (\text{A2})$$

Substituting Eq. (5) into Eqs. (A1) and (A2), we obtain  $\lambda_x$ ,  $\lambda_y$ , and  $\lambda_z$  for arbitrary  $\tau$  [33]:

$$\lambda_x = \frac{\alpha\tau}{2} \left[ 1 + \sum_{\substack{k_d \in K_d \\ k_d \neq k_q}} \text{sinc}(\Delta_{k_d k_q} \tau) \right], \quad (\text{A3})$$

$$\lambda_y = -\frac{\alpha\tau}{2} \sum_{k_d \in \gamma} \sin\left(\frac{\Delta_{k_d k_q} \tau}{2}\right) \text{sinc}\left(\frac{\Delta_{k_d k_q} \tau}{2}\right), \quad (\text{A4})$$

$$\begin{aligned} \lambda_z = \frac{\alpha^2 \tau}{4} & \left[ \sum_{k_d \in \gamma} \frac{\cos(\Delta_{k_d k_q} \tau) - \frac{3}{2} \text{sinc}(\Delta_{k_d k_q} \tau)}{\Delta_{k_d k_q}} + \sum_{k_d \in \gamma} \sum_{\substack{j \in K_d \\ j \neq k_q}} \left\{ \frac{\text{sinc}(\Delta_{j k_q} \tau)}{\Delta_{k_d k_q}} + \frac{\text{sinc}[(\Delta_{k_d k_q} + \Delta_{j k_q}) \tau]}{2\Delta_{j k_q}} \right\} \right. \\ & - \sum_{k_d \in K_d} \sum_{j \in \gamma} \frac{\text{sinc}[(\Delta_{k_d k_q} + \Delta_{j k_q}) \tau]}{2\Delta_{j k_q}} - \sum_{k_d \in \gamma} \sum_{\substack{j \in K_d \\ j \neq k_q \\ j \neq k_d}} \left\{ \frac{1}{\Delta_{k_d k_q}} + \frac{1}{\Delta_{j k_q}} \right\} \frac{\text{sinc}(\Delta_{k_d j} \tau)}{2} \left. \right]. \quad (\text{A5}) \end{aligned}$$

For  $\tau \neq m\tau_0/2$ , terms proportional to the sinc func-

tion remain nonzero. In particular, the remaining

$\text{sinc}(\Delta_{k_d k_q} \tau)$  terms appearing in the summation in Eq. (A3) cannot be suppressed by AIS, thereby reducing its effectiveness. By contrast, these terms vanish for  $\tau = m\tau_0/2$  because  $\sin(n\Delta\tau_0) = 0$  and  $\sin(n\frac{\Delta\tau_0}{2}) = 0$

for all integers  $n$ . The explicit forms of  $\lambda_x$ ,  $\lambda_y$ , and  $\lambda_z$  for  $\tau = m\tau_0/2$ , shown in Eqs. (11)–(13), are obtained by substituting  $\alpha = -\phi/\tau$  and  $\tau = m\tau_0/2$  into Eqs. (A3)–(A5).

---

[1] Y. Nakamura, Y. A. Pashkin, and J. S. Tsai, Coherent control of macroscopic quantum states in a single-Cooper-pair box, *Nature* **398**, 786 (1999).

[2] A. Blais, R.-S. Huang, A. Wallraff, S. M. Girvin, and R. J. Schoelkopf, Cavity quantum electrodynamics for superconducting electrical circuits: An architecture for quantum computation, *Phys. Rev. A* **69**, 062320 (2004).

[3] J. Koch, T. M. Yu, J. Gambetta, A. A. Houck, D. I. Schuster, J. Majer, A. Blais, M. H. Devoret, S. M. Girvin, and R. J. Schoelkopf, Charge-insensitive qubit design derived from the Cooper pair box, *Phys. Rev. A* **76**, 042319 (2007).

[4] L. DiCarlo, J. M. Chow, J. M. Gambetta, L. S. Bishop, B. R. Johnson, D. I. Schuster, J. Majer, A. Blais, L. Frunzio, S. M. Girvin, and R. J. Schoelkopf, Demonstration of two-qubit algorithms with a superconducting quantum processor, *Nature* **460**, 240 (2009).

[5] M. Steffen, D. P. DiVincenzo, J. M. Chow, T. N. Theis, and M. B. Ketchen, Quantum computing: An IBM perspective, *IBM J. Res. Dev.* **55**, 13:1 (2011).

[6] Y. Zhao, Y. Ye, H.-L. Huang, Y. Zhang, D. Wu, H. Guan, Q. Zhu, Z. Wei, T. He, S. Cao, F. Chen, T.-H. Chung, H. Deng, D. Fan, M. Gong, *et al.*, Realization of an error-correcting surface code with superconducting qubits, *Phys. Rev. Lett.* **129**, 030501 (2022).

[7] D. Bluvstein, S. J. Evered, A. A. Geim, S. H. Li, H. Zhou, T. Manovitz, S. Ebadi, M. Cain, M. Kalinowski, D. Hangleiter, J. P. Bonilla Ataides, N. Maskara, I. Cong, X. Gao, P. Sales Rodriguez, *et al.*, Logical quantum processor based on reconfigurable atom arrays, *Nature* **626**, 58 (2024).

[8] A. Anferov, S. P. Harvey, F. Wan, J. Simon, and D. I. Schuster, Superconducting qubits above 20 GHz operating over 200 mK, *PRX Quantum* **5**, 030347 (2024).

[9] S. Konno, W. Asavanant, F. Hanamura, H. Nagayoshi, K. Fukui, A. Sakaguchi, R. Ide, F. China, M. Yabuno, S. Miki, H. Terai, K. Takase, M. Endo, P. Marek, R. Filip, *et al.*, Logical states for fault-tolerant quantum computation with propagating light, *Science* **383**, 289 (2024).

[10] P. W. Shor, Polynomial-time algorithms for prime factorization and discrete logarithms on a quantum computer, *SIAM Rev.* **41**, 303 (1999).

[11] A. W. Harrow, A. Hassidim, and S. Lloyd, Quantum algorithm for linear systems of equations, *Phys. Rev. Lett.* **103**, 150502 (2009).

[12] Y. Sato, H. Tezuka, R. Kondo, and N. Yamamoto, Quantum algorithm for partial differential equations of non-conservative systems with spatially varying parameters, *Phys. Rev. Appl.* **23**, 014063 (2025).

[13] F. Arute, K. Arya, R. Babbush, D. Bacon, J. C. Bardin, R. Barends, R. Biswas, S. Boixo, F. G. S. L. Bradao, D. A. Buell, B. Burkett, Y. Chen, Z. Chen, B. Chiaro, R. Collins, *et al.*, Quantum supremacy using a programmable superconducting processor, *Nature* **574**, 505 (2019).

[14] Google Quantum AI and Collaborators, Quantum error correction below the surface code threshold, *Nature* **638**, 920 (2025).

[15] T. He, W. Lin, R. Wang, Y. Li, J. Bei, J. Cai, S. Cao, D. Chen, K. Chen, X. Chen, Z. Chen, Z. Chen, W. Chu, H. Deng, *et al.*, Experimental quantum error correction below the surface code threshold via all-microwave leakage suppression, *Phys. Rev. Lett.* **135**, 260601 (2025).

[16] A. G. Fowler, M. Mariantoni, J. M. Martinis, and A. N. Cleland, Surface codes: Towards practical large-scale quantum computation, *Phys. Rev. A* **86**, 032324 (2012).

[17] D. Litinski, A game of surface codes: Large-scale quantum computing with lattice surgery, *Quantum* **3**, 128 (2019).

[18] J. M. Hornibrook, J. I. Colless, I. D. Conway Lamb, S. J. Pauka, H. Lu, A. C. Gossard, J. D. Watson, G. C. Gardner, S. Fallahi, M. J. Manfra, and D. J. Reilly, Cryogenic control architecture for large-scale quantum computing, *Phys. Rev. Appl.* **3**, 024010 (2015).

[19] S. Krinner, S. Storz, P. Kurpiers, P. Magnard, J. Heinssoo, R. Keller, J. Luetolf, C. Eichler, and A. Wallraff, Engineering cryogenic setups for 100-qubit scale superconducting circuit systems, *EPJ Quantum Technol.* **6**, 2 (2019).

[20] J. P. G. van Dijk, E. Charbon, and F. Sebastian, The electronic interface for quantum processors, *Micropress. Microsyst.* **66**, 90 (2019).

[21] X. Xue, B. Patra, J. P. G. van Dijk, N. Samkharadze, S. Subramanian, A. Corra, B. Paquet Wuetz, C. Jeon, F. Sheikh, E. Juarez-Hernandez, B. P. Esparza, H. Ramprawala, B. Carlton, S. Ravikumar, C. Nieva, *et al.*, CMOS-based cryogenic control of silicon quantum circuits, *Nature* **593**, 205 (2021).

[22] N. Takeuchi, T. Yamae, T. Yamashita, T. Yamamoto, and N. Yoshikawa, Microwave-multiplexed qubit controller using adiabatic superconductor logic, *npj Quantum Inf.* **10**, 53 (2024).

[23] P. Zhao, R. Wang, M.-J. Hu, T. Ma, P. Xu, Y. Jin, and H. Yu, Baseband control of superconducting qubits with shared microwave drives, *Phys. Rev. Appl.* **19**, 054050 (2023).

[24] N. Takeuchi, T. Yamae, W. Luo, F. Hirayama, T. Yamamoto, and N. Yoshikawa, Scalable flux controllers using adiabatic superconductor logic for quantum processors, *Phys. Rev. Res.* **5**, 013145 (2023).

[25] H. Shen, N. Takeuchi, Y. Yamanashi, and N. Yoshikawa, Amplitude-controllable microwave pulse generator using single-flux-quantum pulse pairs for qubit control, *Supercond. Sci. Technol.* **36**, 095010 (2023).

[26] R. Ohira, R. Matsuda, H. Shiomi, K. Ogawa, and M. Negoro, Optimizing multi-tone microwave pulses via phase selection for quantum computing applications, *J. Appl. Phys.* **136**, 114402 (2024).

[27] R. Menta, F. Cioni, R. Aiudi, M. Polini, and V. Giovan-

netti, Globally driven superconducting quantum computing architecture, *Phys. Rev. Res.* **7**, L012065 (2025).

[28] J. P. G. Van Dijk, B. Patra, S. Subramanian, X. Xue, N. Samkharadze, A. Corna, C. Jeon, F. Sheikh, E. Juarez-Hernandez, B. P. Esparza, H. Rampurawala, B. R. Carlton, S. Ravikumar, C. Nieva, S. Kim, *et al.*, A scalable cryo-CMOS controller for the wideband frequency-multiplexed control of spin qubits and transmons, *IEEE J. Solid-State Circuits* **55**, 2930 (2020).

[29] R. Huang, X. Geng, X. Wu, G. Dai, L. Yang, J. Liu, and W. Chen, Cryogenic multiplexing control chip for a superconducting quantum processor, *Phys. Rev. Appl.* **18**, 064046 (2022).

[30] M. Bakr, Dynamic Josephson-junction metasurfaces for multiplexed control of superconducting qubits, *Phys. Rev. Appl.* **24**, 054069 (2025).

[31] J. P. G. van Dijk, E. Kawakami, R. N. Schouten, M. Veldhorst, L. M. K. Vandersypen, M. Babaie, E. Charbon, and F. Sebastian, Impact of classical control electronics on qubit fidelity, *Phys. Rev. Appl.* **12**, 044054 (2019).

[32] R. Matsuda, R. Ohira, T. Sumida, H. Shiomi, A. Machino, S. Morisaka, K. Koike, T. Miyoshi, Y. Kurihara, Y. Sugita, Y. Ito, Y. Suzuki, P. A. Spring, S. Wang, S. Tamate, *et al.*, Selective excitation of superconducting qubits with a shared control line through pulse shaping, *Phys. Rev. Res.* **8**, L012003 (2026).

[33] H. Mitarai, Y. Tadokoro, and H. Tanaka, Orthogonal frequency-division multiplexing for simultaneous gate operations on multiple qubits via a shared control line, [arXiv:2511.16855](https://arxiv.org/abs/2511.16855) (2025).

[34] B. Chiaro and Y. Zhang, Active leakage cancellation in single qubit gates, *Phys. Rev. Lett.* **135**, 130601 (2025).

[35] R. Wang, P. Zhao, Y. Jin, and H. Yu, Control and mitigation of microwave crosstalk effect with superconducting qubits, *Appl. Phys. Lett.* **121**, 152602 (2022).

[36] D. C. McKay, C. J. Wood, S. Sheldon, J. M. Chow, and J. M. Gambetta, Efficient Z gates for quantum computing, *Phys. Rev. A* **96**, 022330 (2017).

[37] R. W. Chang, Synthesis of band-limited orthogonal signals for multichannel data transmission, *Bell Labs Tech. J.* **45**, 1775 (1966).

[38] T. Hwang, C. Yang, G. Wu, S. Li, and G. Ye Li, OFDM and its wireless applications: A survey, *IEEE Trans. Veh. Technol.* **58**, 1673 (2009).

[39] J. G. Andrews, S. Buzzi, W. Choi, S. V. Hanly, A. Lozano, A. C. K. Soong, and J. C. Zhang, What will 5G be?, *IEEE J. Sel. Areas Commun.* **32**, 1065 (2014).

[40] L. H. Pedersen, N. M. Møller, and K. Mølmer, Fidelity of quantum operations, *Phys. Lett. A* **367**, 47 (2007).

[41] W. Magnus, On the exponential solution of differential equations for a linear operator, *Commun. Pure Appl. Math.* **7**, 649 (1954).

[42] F. Motzoi, J. M. Gambetta, P. Rebentrost, and F. K. Wilhelm, Simple pulses for elimination of leakage in weakly nonlinear qubits, *Phys. Rev. Lett.* **103**, 110501 (2009).

[43] J. M. Gambetta, F. Motzoi, S. T. Merkel, and F. K. Wilhelm, Analytic control methods for high-fidelity unitary operations in a weakly nonlinear oscillator, *Phys. Rev. A* **83**, 012308 (2011).

[44] N. Lambert, E. Giguère, P. Menczel, B. Li, P. Hopf, G. Suárez, M. Gali, J. Lishman, R. Gadhvi, R. Agarwal, A. Galicia, N. Shammah, P. Nation, J. R. Johansson, S. Ahmed, *et al.*, QuTiP 5: The quantum toolbox in Python, [arXiv:2412.04705](https://arxiv.org/abs/2412.04705) (2024).